



The role of REE^{3+} in the crystallization of lanthanites

JUAN DIEGO RODRIGUEZ-BLANCO^{1,2,*}, BEATRIZ VALLINA¹, JESUS A. BLANCO³ AND LIANE G. BENNING^{1,4}

¹ Cohen Geochemistry Laboratory, School of Earth and Environment, University of Leeds, Leeds LS2 9JT, UK

² Nano-Science Center, Department of Chemistry, University of Copenhagen, DK 2100 Copenhagen, Denmark

³ Departamento de Física, Universidad de Oviedo, Oviedo, E-33007, Spain

⁴ GFZ German Research Centre for Geosciences, Helmholtz Centre Potsdam, Telegrafenberg, 14473 Potsdam, Germany

[Received 6 May 2014; Accepted 6 November 2014; Associate Editor: T. Stawski]

ABSTRACT

The formation of crystalline rare earth element (REE) (e.g. La, Ce, Pr, Nd) carbonates from aqueous solutions was examined at ambient temperature using UV-Vis spectrophotometry, combined with X-ray diffraction, high-resolution microscopy and infrared spectroscopy. In all experiments REE -lanthanites ($REE_2(CO_3)_3 \cdot 8H_2O$) formed *via* a highly hydrated, nanoparticulate and poorly-ordered REE -carbonate precursor. The lifetime of this precursor as well as the kinetics of crystallization of the various REE -lanthanites were dependent on the specific REE^{3+} ion involved in the reaction. The induction time and the time needed to fully form the crystalline REE -lanthanite end products increase linearly with the ionic potential. The authors show here that the differences in ion size and ionic potential as well as differences in dehydration energy of the REE^{3+} ions control the lifetime of the poorly ordered precursor and thus also the crystallization kinetics of the REE -lanthanites; furthermore, they also affect the structural characteristics (e.g. unit-cell dimensions and idiomorphism) of the final crystalline lanthanites.

KEYWORDS: lanthanite, REE , ionic potential, carbonatite, crystallization, amorphous precursors.

Introduction

RARE-EARTH ELEMENT carbonates are important groups of compounds usually found in carbonatite deposits (e.g. Bayan Obo, China; Mountain Pass, USA; Castor and Hedrick, 2006). Their consumption is considered an economic indicator, as REE are essential for modern technological applications (electronics, renewable energy technologies, magnets, lasers, etc.). Strong demand for several REE (e.g. La, Nd, Eu, Dy) exists at present and as electronic usage expands in the coming decades this is expected to increase further (Bauer *et al.*, 2011).

Two of the most important minerals in such deposits are lanthanites ($REE_2(CO_3)_3 \cdot 8H_2O$) and bastnäsites ($REE(OH,F)CO_3$), which include La,

Ce, Pr and Nd as major elements but also often traces of heavier rare-earths (e.g. Sm, Eu, Dy). REE -lanthanites consist of layers of 10-fold coordinated REE -O polyhedra and CO_3 groups connected by hydrogen bonds to interlayer water molecules, forming a highly hydrated mineral structure (Morrison *et al.*, 2013). Most research to date has focused on the structural determination and the crystal chemistry of natural samples from different ores, with results suggesting that REE -lanthanites are compositionally highly variable (e.g. Graham *et al.*, 2007 and references therein). This compositional variability points towards dissimilar conditions during their formation or to

* E-mail: jblanco@nano.ku.dk
DOI: 10.1180/minmag.2014.078.6.03

This paper is published as part of a special issue in *Mineralogical Magazine*, Vol. 78(6), 2014 entitled 'Mineral–fluid interactions: scaling, surface reactivity and natural systems'.

variations in *REE* source (weathering, hydrothermal, *etc.*). There is no information about the crystallization mechanisms of *REE*-lanthanites or about the mobility and fate of the rare-earth elements during their formation, however. The factors promoting or inhibiting the crystallization and stability of these minerals are not known. This leads to the following questions: do *REE*-lanthanites crystallize like other divalent metal carbonates (e.g. Ca^{2+} or Mg^{2+} ; Rodriguez-Blanco *et al.*, 2011, 2014), or like trivalent metal (e.g. Fe^{3+} or Al^{3+} ; Roncal-Herrero *et al.*, 2009) or *REE* phosphates (e.g. La^{3+} or Nd^{3+} ; Roncal-Herrero *et al.*, 2011), through the breakdown of poorly ordered, nanoparticulate and highly hydrated precursors? Or, do they form through oriented attachment of nanocrystalline particles akin to other salt systems (e.g. gypsum: Van Driessche *et al.*, 2012; hematite: Niederberger *et al.*, 2002; fluorapatite: Simon *et al.*, 2004; or calcite: Niederberger and Cölfen, 2006 and references therein)? Lastly, is the crystallization kinetics of *REE*-lanthanites dependent on the REE^{3+} ionic radius as observed in the CaCO_3 - MgCO_3 system (Bischoff, 1968)? Answering these questions would shed light on the origin of *REE*-bearing carbonate minerals, as well as perhaps provide insight into the mobility of *REE* under natural conditions.

In the present study, *in situ* and real-time UV-Vis spectrophotometric measurements in solution were combined with the characterization of the solids by X-ray diffraction (XRD), infrared (IR) spectroscopy and imaging and the kinetics of crystallization of La, Ce, Pr and Nd lanthanites from REE^{3+} solutions were studied. The results suggest that at high supersaturations all *REE*-lanthanites form *via* an amorphous precursor and that the ionic potential of the REE^{3+} ions (i.e. the ion's charge density, calculated by dividing the valence of the REE^{3+} by its ionic radius) controls the precursor stability and kinetics of crystallization, as well as the crystal characteristics of the endmember *REE*-lanthanites.

Experimental

REE carbonates (*REE* = La, Ce, Pr, Nd) were synthesized individually by mixing a 10 mM solution of the relevant $\text{REE}(\text{NO}_3)_3 \cdot 6\text{H}_2\text{O}$ (Alfa Aesar, 99.9% purity) with a 10 mM Na_2CO_3 solution (Fisher Scientific, 99.9% purity) at 21°C under constant and continuous stirring. Immediately after mixing, in all cases, a relatively

translucent suspension formed. The transformation of these initial precipitates was followed *in situ* and in a time-resolved manner through the development of turbidity in solutions that were mixed directly in a 2 ml cuvette set in a stirred module of a double beam UV-VIS spectrometer (Uvikon XL, SECOMAN Ltd). Changes in absorption at 450 nm were recorded every second for up to 17 h. The initial precipitates as well as the end-product solids were vacuum filtered (0.2 μm), washed with water and isopropanol and dried following the method described by Rodriguez-Blanco *et al.* (2008). All solid phases were characterized by powder X-ray diffraction (PXRD) using a Bruker D8 X-ray Diffractometer ($\text{CuK}\alpha 1$, $5-70^\circ 2\theta$, $0.001^\circ/\text{step}$; 0.1 or 1 s/step). The unit-cell parameters and full-width at half-maximum (FWHM) of the (002) Bragg peak of lanthanite were determined with the *TOPAS* software (Coelho, 2003), using the Shinn and Eick (1968) model for the lanthanite structure (ICSD-22224). Images of the initial precipitate and the various *REE*-lanthanite phases were acquired with a field emission gun scanning electron microscope (FEG-SEM, LEO 1530 Gemini, operated at 3 kV and with an in-lens detector). In addition, Fourier transform infrared (FTIR) spectra of the initial precipitates were recorded on an A2-Technology Microlab mid-IR spectrometer with a Diamond internal reflection cell with spectra collected in the $650-4000\text{ cm}^{-1}$ range by co-adding 1024 scans at a resolution of 4 cm^{-1} .

The hydrogeochemical modelling software *PHREEQC* (Parkhurst, 1995, using the LLNL database) was used to determine the initial saturation index of the aqueous solution with respect to lanthanites immediately after mixing of the 10 mM stock solutions and prior to the precipitation of any solid phases. Solubility products data for the amorphous *REE*-bearing carbonates are lacking from the literature and data on crystalline lanthanites are also scarce. Solubility data exist only for lanthanite-(La), lanthanite-(Ce) and lanthanite-(Nd) and the log *K*_{sp} values for these phases are reported as: 13.7, 18.3 and 14.1, respectively (Essington and Mattigod, 1985).

Results and discussion

In all experiments, regardless of REE^{3+} ion used, the precipitates that formed immediately after mixing were characterized by X-ray patterns with

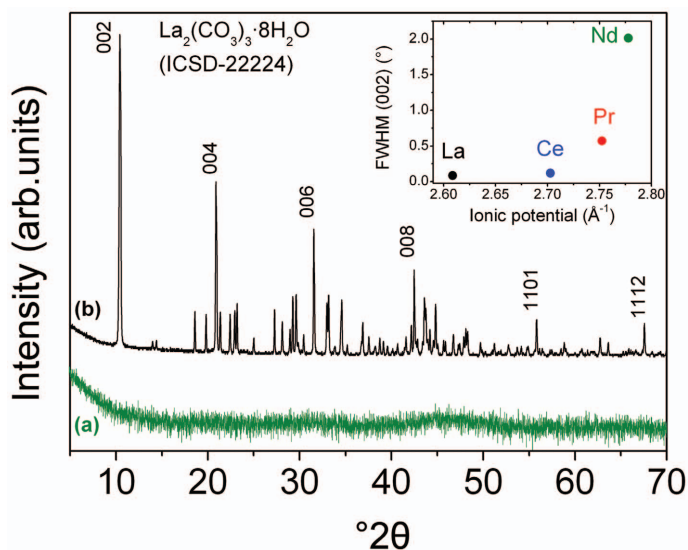


FIG. 1. X-ray diffraction patterns of amorphous Nd carbonate (a) and lanthanite-La (b). Inset: variation of the FWHM of the (002) Bragg peak with ionic potential of the REE³⁺ ions. The PXRD patterns are typical for all poorly ordered REE precursors (a) or crystalline REE-lanthanite end products (b) regardless of REE³⁺ ion.

no Bragg peaks (pattern *a* in Fig. 1) but with three weak and broad bumps, centred around 20, 32 and 45°2θ. The FTIR analysis (Fig. 2) revealed ionic vibrations and bands typical of carbonates (located between 1455 and 679 cm⁻¹) and O–H vibrations (located between 2500 and 3700 cm⁻¹) that corresponded to structural water. The SEM

images showed that all gel-like phases consisted of spherical nanoparticles with diameters of <~50 nm (Fig. 2, inset).

Upon aging of the aqueous suspension for up to ~17 h, all initial amorphous precipitates crystallized to REE-lanthanites (Fig. 1, upper pattern). An in-depth analysis of the PXRD patterns

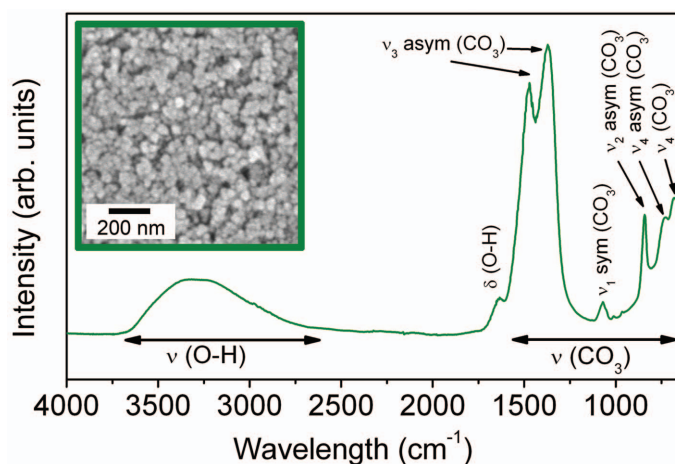


FIG. 2. FTIR spectrum of amorphous Nd carbonate, including band assignments. The image shows the spectrum for Nd carbonate as an example, but FTIR spectra for all initial REE carbonates were similar. Inset: secondary electron SEM image of amorphous Nd carbonate obtained immediately after mixing the aqueous solutions.

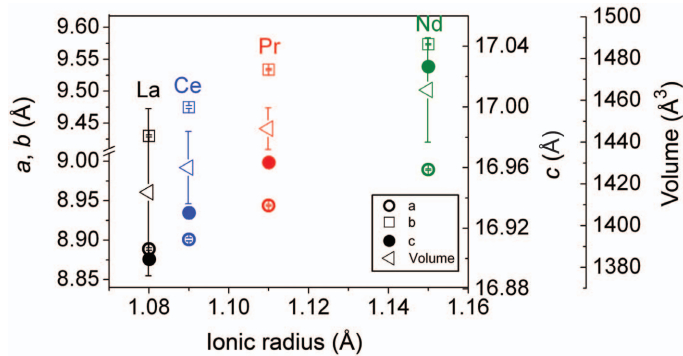


FIG. 3. Variation of the unit-cell parameters and volume of the unit cells of lanthanites (La, Ce, Pr and Nd) as a function of the REE^{3+} ionic radius.

revealed that the unit-cell parameters and volumes of the various REE -lanthanites were proportional to the ionic radius of the respective REE^{3+} ion (Fig. 3; Table 1). However, the FWHM of the lanthanite (002) Bragg peak was proportional to the ionic potential of the REE^{3+} ion (Fig. 1, inset and Table 1), indicating that the lanthanites containing heavier REE^{3+} ions (Nd^{3+} or Pr^{3+}) probably developed smaller crystallite sizes compared to their lighter REE^{3+} -bearing counterparts (La^{3+} or Ce^{3+}). This trend was also reflected in the variations in idiomorphism of the final crystalline solids (Fig. 4). All lanthanites consisted of platy crystals $\sim 5 \mu m$ or smaller in size. However, while the lanthanite-(La) developed well formed and regular euhedral shapes (Fig. 4a), the heavier REE^{3+} -bearing lanthanites (Ce, Pr and Nd) progressively developed more

subhedral shapes with crystal imperfections and/or twinning (Fig 4b–d).

The *in situ* and real-time turbidity data revealed that both the onset of the crystallization (induction time; Fig. 5, star symbols) as well as the end of the crystallization reaction (Fig. 5, diamond symbols) depended on the REE^{3+} ion. Immediately after solution mixing, turbidity values were low (1–2%) but after a REE^{3+} -dependent induction time (e.g. 2 min in the La system, >100 min in the Nd system) the turbidity started to increase, marking the beginning of the crystallization reaction. The shape and slopes of the turbidity curves as well as the maximum turbidity and thus the completion of the crystallization followed a similar pattern. The analysis of these data showed that the induction time and the time needed to fully form the crystalline REE -

TABLE 1. Unit-cell parameters and FWHM of (002) Bragg peak of La-, Ce-, Pr- and Nd-bearing lanthanite end products. Shown in column one (in brackets) are the ionic radii and the ionic potentials of each REE^{3+} ion.

Ion (ionic radii; ionic potential)	<i>a</i> (Å)	<i>b</i> (Å)	<i>c</i> (Å)	Volume (Å ³)	FWHM (002) Bragg peak of REE -Lanthanites (°)
La (1.15 Å; 2.60 Å ⁻¹)	8.989 ± 0.001	9.573 ± 0.001	17.027 ± 0.001	1465.0 ± 25.0	0.085
Ce (1.11 Å; 2.70 Å ⁻¹)	8.944 ± 0.001	9.533 ± 0.001	16.963 ± 0.002	1446.4 ± 10.0	0.119
Pr (1.09 Å; 2.75 Å ⁻¹)	8.901 ± 0.002	9.474 ± 0.002	16.930 ± 0.004	1427.8 ± 17.3	0.570
Nd (1.08 Å; 2.77 Å ⁻¹)	8.889 ± 0.002	9.430 ± 0.002	16.900 ± 0.002	1416.0 ± 40.0	2.014

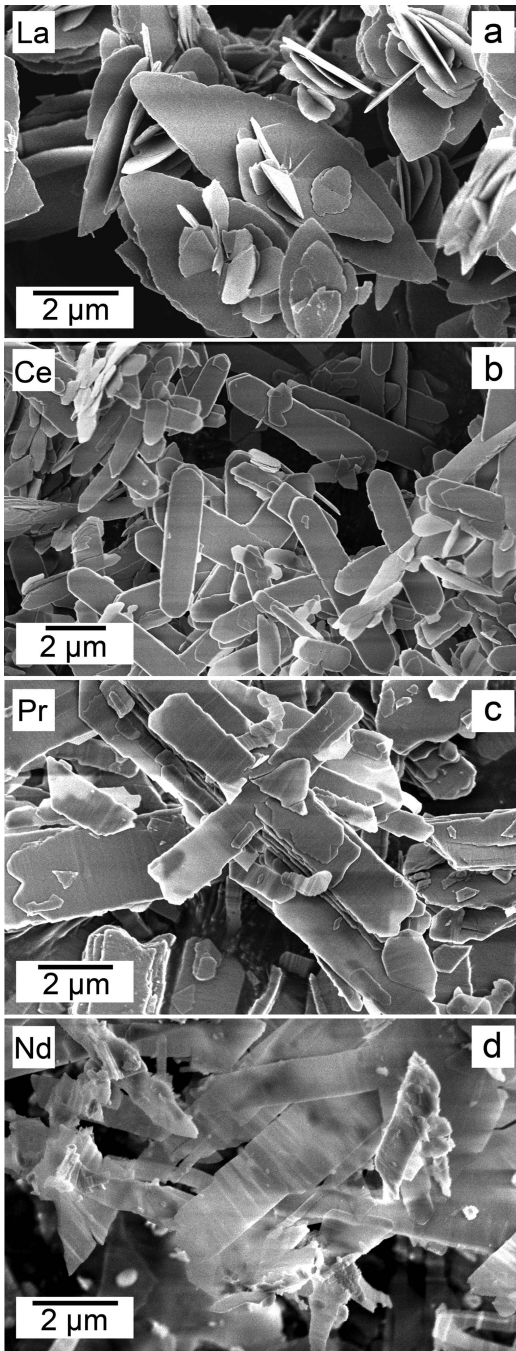


FIG. 4. SEM images of pure REE-lanthanites, where REE corresponds to La (a), Ce (b), Pr (c) and Nd (d).

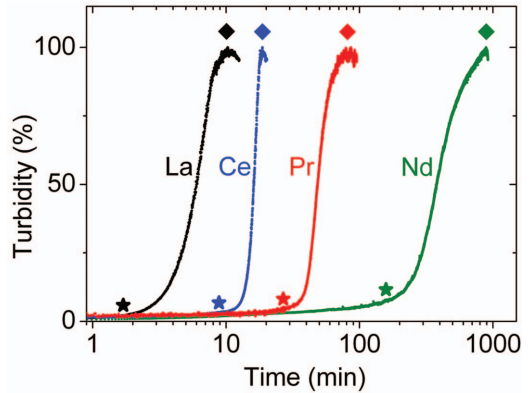


FIG. 5. Turbidity curves from the *in situ* and time-resolved UV-Vis experiments, showing the evolution of the crystallization of REE-lanthanites in aqueous solution at ambient temperature (REE = La, Ce, Pr, Nd).

lanthanite increase linearly with the ionic potential of the REE³⁺ ion (Fig. 6).

The combination of PXRD, SEM and FTIR data suggests that in all cases the REE-lanthanites crystallize through intermediate, poorly ordered and highly hydrated precursors, following a non-classical nucleation pathway (Meldrum and Sear, 2008) as it may also occur to calcium carbonates (e.g. Rodriguez-Blanco *et al.*, 2012, 2014; Bots *et al.*, 2012). The formation of poorly ordered carbonate precursor phases is not unexpected because such poorly ordered precursors form at high supersaturation levels and basic pH. Our calculations with PHREEQC revealed that the

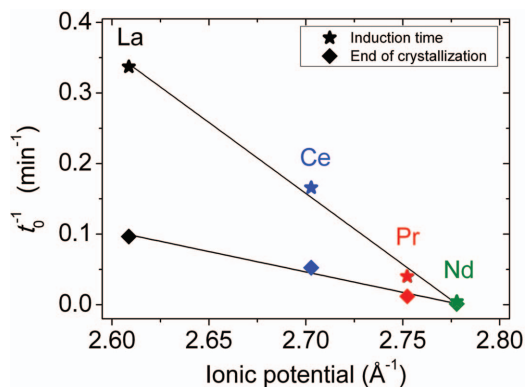


FIG. 6. Plot showing the inverse of the induction time and inverse of time needed to complete the crystallization of the REE-lanthanites as a function of the ionic potential of the REE³⁺ ion.

saturation index values of lanthanite-(La), lanthanite-(Ce) and lanthanite-(Nd) immediately after solution mixing (i.e. before the precipitation of the amorphous precursor) were 11.51, 5.95 and 9.59, respectively, and that the pH after solution mixing was ~8.4.

The linear relationships shown in Fig. 6 suggest that the ionic potential of the REE^{3+} cation controls both the lifetime of the precursor and the crystallization kinetics of the REE -lanthanites. The ionic potential is a measure of an ion's charge density and reflects the strength of the electrostatic attraction to ions of opposite charge (Railsback, 2003). It is calculated by dividing the valence of the ion by its ionic radius (Table 1; Cartledge, 1928*a,b*). Poorly ordered carbonate precursors are often hydrated (Rodriguez-Blanco *et al.*, 2011, 2014; Vallina *et al.*, 2013) and in many cases their crystallization occurs through the progressive loss of structural water within the disordered framework of the amorphous precursor solid (Radha *et al.*, 2010; Goodwin *et al.*, 2010).

The lifetime of the poorly ordered REE^{3+} -bearing precursors and the crystallization kinetics of REE -lanthanites are suggested here to be dependent on the energy needed to dehydrate the REE^{3+} ions in the precursor phase and therefore on the respective REE ionic potential. Thus, the poorly ordered precursors for the greater-ionic potential (i.e. heavier) REE -bearing carbonates require a greater dehydration energy and thus more time than their lower-ionic potential (i.e. lighter) counterparts. This slower dehydration of the heavier REE^{3+} ions is in agreement with the behaviour observed in amorphous Ca-Mg carbonates. We have previously shown that Mg^{2+} -bearing amorphous calcium carbonate (Mg-ACC) is more stable than pure ACC (Rodriguez-Blanco *et al.*, 2012, 2014) and attributed this to the larger energy required to dehydrate the Mg^{2+} ion as also suggested through molecular modelling (e.g. di Tommaso and de Leeuw, 2010). This is because Mg^{2+} has a larger ionic potential (3.07 \AA^{-1}) than the Ca^{2+} ion (2.01 \AA^{-1}). In a similar manner lanthanides with greater ionic potential (e.g. the heavier ions Nd^{3+} , Dy^{3+}) are known to be able to retain more strongly their bonded residual water, even above 700°C , while the lanthanides with lower ionic potential (e.g. La^{3+}) release water at lower temperatures (Fedorov *et al.*, 2002; Vallina *et al.*, 2013). This dependence on ionic potential is also consistent with the observed inverse relationship with crystallite size, because the retention of

residual water bonded to the REE^{3+} ion will invariably be translated into the generation of structural defects during the crystallization process.

Implications

Although additional studies are required to be able to fully predict the mobility and fate of rare-earth elements during the water–rock interaction process, we have nevertheless demonstrated here that various REE -lanthanites can be synthesized through an easy ‘green’ synthesis route using simple aqueous solutions and ambient temperatures. Such simple methods could be useful for re-processing of ores or recycling of materials that contain REE to enhance recovery. Our data also identify the parameters that control kinetically the crystallization of REE -bearing carbonates from solution. Having quantified the main kinetic factors that affect the crystallization of REE -bearing minerals we can assert that at similar saturation levels an assessment of the processes by which such mineral phases are formed and concentrated in geological deposits is now feasible. This knowledge may also help with prospecting approaches to locate new REE deposits and thus diminish the problem of future increased demand for REE required for advanced technological applications.

Acknowledgements

This study was supported by the Marie Curie EU-FP6 Mineral Nucleation and Growth Kinetics (MIN-GRO) Research and Training Network under contract MRTNCT-2006-035488 and the Spanish Ministry of Economy and Competitiveness (MICINN-12-MAT2011-27573-C04-02). The authors thank the Cohen Laboratories in the School of Earth and Environment, the Leeds Electron Microscopy and Spectroscopy Centre (LEMAS) at the Faculty of Engineering (University of Leeds, UK). They also thank Yoshiko Fujita (Idaho National Laboratory), the associate editor and reviewers for their constructive comments which have helped to improve the manuscript.

References

- Bauer, D., Diamond, D., Li, J., McKittrick, M., Sandalow, D. and Telleen, P. (2011) *Critical Materials Strategy*. US Department of Energy.

- Washington, DC, 2011. <http://energy.gov/node/349057>
- Bischoff, J.L. (1968) Kinetics of calcite nucleation: magnesium ion inhibition and ionic strength catalysis. *Journal of Geophysical Research*, **73**, 3315–3322.
- Bots, P., Rodriguez Blanco, J.D., Roncal-Herrero, T., Shaw, S. and Benning, L.G. (2012) Mechanistic insights into the crystallization of amorphous calcium carbonate to vaterite. *Crystal Growth and Design*, **12**, 3806–3814.
- Cartledge, G.H. (1928a) Studies on the periodic system. I. The ionic potential as a periodic function. *Journal of the American Chemical Society*, **50**, 2855–2863.
- Cartledge, G.H. (1928b) Studies on the periodic system. I. The ionic potential and related properties. *Journal of the American Chemical Society*, **50**, 2863–2872.
- Castor, S.B. and Hedrick, J.B. (2006) Rare earth elements. Pp. 769–792 in: *Industrial Minerals and Rocks* (J. Elzea Kogel, N.D. Trivedi and J.M. Barker, editors). Society for Mining, Metallurgy and Exploration, Littleton, Colorado, USA.
- Coelho, A.A. (2003) *TOPAS: General Profile and Structure Analysis Software for Powder Diffraction Data*. Coelho Software, Brisbane, Australia.
- Di Tommaso, D. and De Leeuw, N.H. (2010) Structure and dynamics of the hydrated magnesium ion and of the solvated magnesium carbonates: insights from first principles simulations. *Physical Chemistry Chemical Physics*, **12**, 894–901.
- Essington, M.E. and Mattigod, S.V. (1985) Lanthanide solid phase speciation. *Soil Science Society of America Journal*, **49**, 1387–1393.
- Fedorov, P.P., Nazarkin, M.V. and Zakalyukin, R.M. (2002) On polymorphism and morphotropism of rare earth sesquioxides. *Crystallography Reports*, **47**, 281–286.
- Goodwin, A.L., Michel, F.M., Phillips, B.L., Keen, D.A., Dove, M.T. and Reeder, R.J. (2010) Nanoporous structure and medium-range order in synthetic amorphous calcium carbonate. *Chemistry of Materials*, **22**, 3197–3205.
- Graham, I.T., Pogson, R.E., Colchester, D.M., Hergt, J., Martin, R. and Williams, P.A. (2007) Pink lanthanite-(Nd) from Whitianga Quarry, Coromandel Peninsula, New Zealand. *The Canadian Mineralogist*, **45**, 1389–1396.
- Meldrum, F.C. and Sear, R.P. (2008) Now you see them. *Science*, **322**, 1802–1803.
- Morrison, S.M., Andrade, M.B., Wenz, M.D., Domanik, K.J. and Downs, R.T. (2013) Lanthanite-(Nd), Nd₂(CO₃)₃·8H₂O. *Acta Crystallographica*, **E69**, i15–i16.
- Niederberger, M. and Cölfen, H. (2006) Oriented attachment and mesocrystals: Non-classical crystallization mechanisms based on nanoparticle assembly. *Physical Chemistry Chemical Physics*, **8**, 3271–3287.
- Niederberger, M., Krumeich, F., Hegetschweiler, K. and Nesper, R. (2002) An iron polyolate complex as a precursor for the controlled synthesis of mono-dispersed iron oxide colloids. *Chemistry of Materials*, **14**, 78–82.
- Parkhurst, D.L. (1995) *User's guide to PHREEQC – A computer program for speciation, reaction-path, advective-transport, and inverse geochemical calculations*. U.S. Geological Survey Water-Resources Investigations Report 95-4227, 143 pp.
- Radha, A.V., Forbes, T.Z., Killian, C.E., Pupa, G. and Navrotsky, A. (2010) Transformation and crystallization energetics of synthetic and biogenic amorphous calcium carbonate. *Proceedings of the National Academy of Sciences USA*, **107**, 16348–16443.
- Railsback, L.B. (2005) A synthesis of systematic mineralogy. *American Mineralogist*, **90**, 1033–1041.
- Rodriguez-Blanco, J.D., Shaw, S. and Benning, L.G. (2008) How to make 'stable' ACC: protocol and preliminary structural characterization. *Mineralogical Magazine*, **72**, 283–286.
- Rodriguez-Blanco, J.D., Shaw, S. and Benning, L.G. (2011) The kinetics and mechanisms of amorphous calcium carbonate (ACC) crystallization to calcite, via vaterite. *Nanoscale*, **3**, 265–271.
- Rodriguez-Blanco, J.D., Shaw, S., Bots, P., Roncal-Herrero, T. and Benning, L.G. (2012) The role of pH and Mg on the stability and crystallization of amorphous calcium carbonate. *Journal of Alloys and Compounds*, **536**, S477–S479.
- Rodriguez-Blanco, J.D., Shaw, S., Bots, P., Roncal-Herrero, T. and Benning, L.G. (2014) The role of Mg in the crystallisation of monohydrocalcite. *Geochimica et Cosmochimica Acta*, **127**, 204–220.
- Roncal-Herrero, T., Rodriguez-Blanco, J.D., Benning, L.G. and Oelkers, E.H. (2009) Precipitation of iron and aluminium phosphates directly from aqueous solution as a function of temperature from 50 to 200°C. *Crystal Growth & Design*, **9**, 5197–5205.
- Roncal-Herrero, T., Rodriguez-Blanco, J.D., Oelkers, E.H. and Benning, L.G. (2011) The direct precipitation of rhabdophane (REEPO₄·nH₂O) nano-rods from acidic aqueous solutions at 5–100°C. *Journal of Nanoparticle Research*, **13**, 4049–4062.
- Shinn, D.B. and Eick, H.A. (1968) The crystal structure of lanthanum carbonate octahydrate. *Inorganic Chemistry*, **7**, 1340–1345.
- Simon, P., Carrillo-Cabrera, W., Formánek, P., Göbel, C., Geiger, D., Ramlau, R., Tlatlik, H., Buder, J. and Knip, R. (2004) On the real-structure of biomimetically grown hexagonal prismatic seeds of fluorapatite-gelatine-composites: TEM investigations

- along [001]. *Journal of Materials Chemistry*, **14**, 2218–2224.
- Vallina, B., Rodriguez-Blanco, J.D., Blanco, J.A. and Benning, L.G. (2013) Amorphous dysprosium carbonate: characterization, stability and crystallization pathways. *Journal of Nanoparticle Research*, **15**, 1438.
- Van Driessche, A.E.S., Benning, L.G., Rodriguez-Blanco, J.D., Ossorio, M., Bots, P. and García-Ruiz, J.M. (2012) The role and implications of bassanite as a stable precursor phase to gypsum precipitation. *Science*, **336**, 69–72.